

Nanoelectrodes: energy conversion and storage

Materials take on exceptional properties as we enter the nanodomain and Electromaterials: those that transport and/or transfer charge are no exception. As such the ability to impart nanostructure to electrodes is having a dramatic effect on areas such as energy conversion and storage.

Gordon G. Wallace^{1,*}, Jun Chen¹, Attila J. Mozer¹, Maria Forsyth², Douglas R. MacFarlane², Caiyun Wang¹

¹ARC Centre of Excellence for Electromaterials Science, Intelligent Polymer Research Institute, University of Wollongong, Wollongong, NSW 2522, Australia.

²ARC Centre of Excellence for Electromaterials Science, Monash University, Clayton, VIC 2800, Australia.

*Email: gwallace@uow.edu.au

Nanosized materials are known to take on peculiar properties compared to the bulk material. Their electronic and mechanical properties are known to improve e.g. higher electrical conductivity and greater strength. Their electrochemical redox properties can change dramatically, e.g. in the case of Ag° , the E° value for $\text{Ag}^{\circ} \rightarrow \text{Ag}^{+} + e$ can change by up to half a volt as the particle size decreases. Nanodimensional materials also have an extraordinarily high surface area to volume ratio. All of these properties would bring beneficial effects if they could be retained when the material is assembled into a structure capable of being used as an electrode – nanostructured electrodes.

Here we consider selected examples illustrating the importance of nanostructured electrodes in energy conversion (organic solar cells and fuel cells) and storage (batteries and capacitors). These examples involve the use of inorganic as well as organic conducting and semiconducting materials.

Solar cells

If the energy needs of our rapidly growing population continue to expand at the current pace, a significantly larger fraction of our energy supply will need to be sourced from renewable sources in the very

near future¹. The projected energy shortage by 2050 is often referred to as the “terawatt” challenge². In comparison to any other energy sources currently available, the sun delivers a continuous energy current of around 1.7×10^{17} W (1.5×10^{18} kWh/year), which exceeds approximately by four orders of magnitude the current annual global energy consumption (10^{14} kWh/year)³. Due to this simple fact and an increasing public concern about green house gas emission and its impact on climate, research into solar cells that efficiently convert the sun’s energy into electricity has accelerated. Completely new solar cell architectures have been discovered that use organic materials (polymers and pigments) that were more conventionally used as, for example, passive insulating materials in electronics, fillers or pigments in paints. These innovations would not have been possible without the development of various nanofabrication and characterization tools.

The two most efficient organic photovoltaic architectures to date are the polymer bulk heterojunction solar cells (BHSC)⁴ and the dye-sensitized solar cells (DSSC)⁵. These are schematically displayed in Fig. 1. The main structural feature of both of these solar cells is the interpenetrating network of an electron donor (and transporter) and an electron acceptor (and transporter) material. In BHSC, the photon absorption by the conjugated polymer (e.g. polythiophenes P3HT⁶

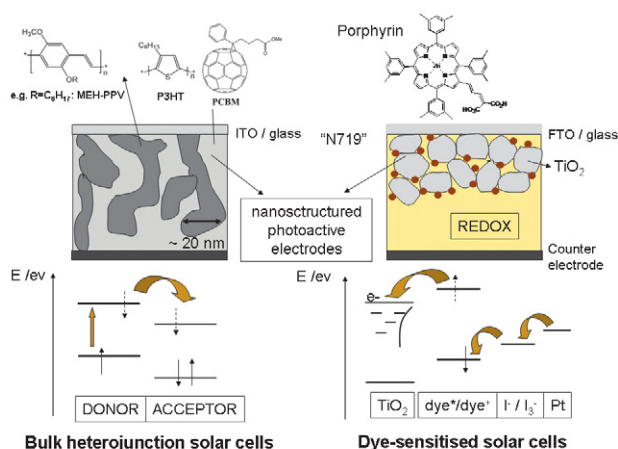


Fig. 1 Schematic representations of the i) nanostructured photoactive electrodes used in organic solar cells, ii) chemical structures of the most commonly used materials used to construct them; and iii) energy diagrams depicting the various photo-induced electron transfer processes.

or polyphenylene-vinylenes⁷, PPV) leads to exciton migration to the interface with the acceptor where charge injection into an unoccupied molecular orbital of the acceptor (typically a solubilised fullerene molecule, PCBM) occurs. Since the typical exciton diffusion length for singlet excited states is around 5-10 nm⁸, the maximum domain size of the electron donor is limited to around 20 nm. This can only be achieved by a fine control over the nanostructure of the donor/acceptor phase-separated interpenetrating network. However, this presents another challenge: a large surface area where the electron and hole conducting phases are in intimate contact, increasing the chance of recombination.

In DSSCs, a strongly light absorbing pigment, for example, ruthenium complexes⁹ or porphyrins¹⁰, is chemically attached to an inorganic wide band gap semiconductor such as TiO₂¹¹. Charge separation occurs by photoinduced electron injection from the dye excited state into the conduction band of the oxide. Since the absorption cross-section of a dye molecule is much smaller than the area occupied on the semiconductor surface, a large surface area (mesoscopic or nanoporous) electrode is required. In the most efficient DSSCs, surface roughness (internal surface area projected to the geometric surface area) of 1000 has been realized¹². This ensures that nearly all photons incident on the sample in the absorption range of the dye are absorbed. The photo-oxidised dye is reduced by a redox mediator which is then regenerated on a catalytically active counter electrode.

The use of a nanostructured inorganic oxide electrode ensures a large internal surface area and this is critical in achieving efficient light harvesting (DSSC) and charge separation (BHSC).

Bulk heterojunction solar cells

The first bulk heterojunction solar cells were prepared by a simple mixing of the donor/acceptor components in a common solvent, followed by deposition on the conductive transparent glass by spin coating⁷, providing little control over the phase separated morphology¹³. Treatment of the deposited material using procedures such as heating/⁶ electric bias and solvent vapor treatment¹⁴ have all been shown to modify the nanostructure leading to better performance and/or stability. More recently, intelligent molecular design of the donor/acceptor constituents achieved well-defined, tunable and reproducible morphologies. Some recent design concepts are displayed in Fig. 2.

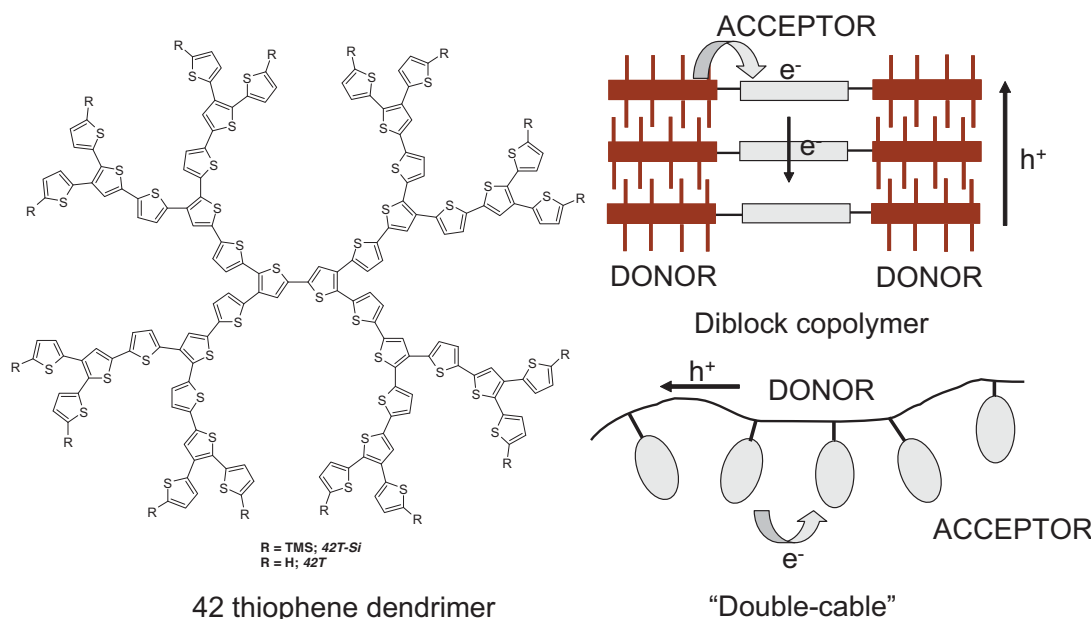


Fig. 2 Nanostructure control at the molecular levels: Some recent examples of novel donor / acceptor materials with intelligent molecular design.

- It was demonstrated that shape-persistent, monodisperse, hyperbranched thiophene dendrimer donors of up to the 4th generation (90 thiophene units) can be prepared using highly controlled synthetic approaches¹⁵. The primary scale of phase separation was proposed to be the size of the dendrimer macromolecule, which is then tunable depending on the generation (and number of connected thiophene units) used. A clear correlation between the dendrimer generation and the photovoltaic response has been shown¹⁶.
- All-conjugated donor/acceptor diblock copolymers were shown to form well-defined, nanosized supramolecular structures¹⁷. The phase separation, and therefore diffusion length of excitons, can be controlled by the block size.
- Main chain conjugated donor cables with side chain attached acceptors (so called "double-cables") were synthesized¹⁸. It is envisaged that after charge separation the positive charge travels along the conjugated polymer backbone and the electrons travel by "hopping" transport between adjacent acceptor moieties¹⁹.

Dye-sensitized solar cells

Dye-sensitized photoanodes typically consist of a nanostructured electrode which provides high surface area for dye binding; essential for efficient light harvesting. In the most commonly used configuration the photoanode consists of 10 – 30 nm primary size anatase TiO₂ nanocrystals that are deposited in a mixture containing an organic binder. After high temperature sintering the binder is removed leaving behind a highly porous (porosity around 50–60%) electrode with interconnected TiO₂ particles. This simple and cost effective fabrication method results in record DSSCs efficiencies in conventional liquid-type DSSCs of 11%²⁰. There are two main fundamental reasons to depart from this rather straightforward and efficient fabrication: (i) fabrication of photoanodes with even higher internal surface area, dye uptake and consequently, light harvesting; or ii) faster electron transport by creating ordered nanostructures. The latter may be important when the charge separated lifetimes are shorter due to the use of, for example, faster redox shuttles, solids state hole conductors or gel electrolytes.

Caruso *et al.*²¹ have prepared submicron sized TiO₂ nanobeads (830 ± 40 nm) with surface areas up to 108 m².g⁻¹ and tunable pore sizes using a combination of sol-gel and solvothermal synthetic methods. The increased surface area has resulted in an increased dye uptake and consequently, light harvesting efficiency. An efficiency improvement in the order of 25% was demonstrated when compared to photoanodes prepared using commercially available P25 TiO₂ (Degussa-Huls).

In contrast to electron transport in a network of interconnected, randomly oriented TiO₂ nanoparticles, nanotubes^{22,23} and nanowires²⁴ may provide improved electron transport due to less grain boundaries and fewer electron traps. In particular, aligned nanotubes²⁵ that span across the entire length of the photoanode (10–15 μm) providing

the shortest route for electron collection is thought to be beneficial. Kuang *et al.*²⁵ have reported an efficient flexible dye-sensitized solar cell using aligned TiO₂ nanotube arrays with 5–14 μm length and an ionic liquid electrolyte. TiO₂ nanotubes were prepared by electrochemical anodisation of Ti foils, and the thickness of the tubes was controlled by the anodisation time. An impressive 3.6% power conversion efficiency was achieved when 14 μm nanotube photoanodes in combination with a flexible ITO/PEN (polyethylene naphthalate) counter electrodes were used.

A core-shell approach in which a thin (few nm) coating of an inorganic semiconductor is uniformly applied over a nanostructured inorganic semiconductor electrode with different electronic properties (band gap, conduction/valence band potential and doping level) are often used to block unwanted charge recombination reactions²⁶.

For example, an insulating large band gap oxide, such as ZnO, TiO₂, ZrO₂, MgO, Al₂O₃, Y₂O₃ is coated on SnO₂ significantly enhancing its photovoltaic performance²⁷. An increase in dye uptake compared to uncoated SnO₂ is reported, which together with suppressed electron back reactions from the SnO₂ to the acceptor in the redox containing electrolyte, resulted in an impressive 4–5 fold increase in power conversion efficiency (from 1.2% for uncoated SnO₂ electrodes to 5.2% for ZnO/SnO₂ core-shell structures). It was proposed that the sub-nm (0.1 nm to 0.59 nm) coatings are sufficiently thin to achieve efficient electron injection by tunneling through the insulating barrier layer, yet provide insulation of the surface to suppress electron recombination.

Atomic layer deposition²⁸ (ALD) appears to be a method of great benefit to achieve precisely controlled, conformal, uniform nanoscale coatings. For example, Law *et al.*²⁴ have demonstrated that the thickness of the Al₂O₃ or TiO₂ shell on ZnO nanowire arrays can be controlled simply by the number of ALD cycles applied. A clear correlation between the number of ALD layers and the DSSC performance has been demonstrated. In case of Al₂O₃/ZnO structure, a blocking of both recombination current and electron injection has been found, the latter dominating the response resulting in lower overall power conversion efficiency. The TiO₂/ZnO structure, on the other hand, proved to be superior to the uncoated ZnO nanowire cell increasing the efficiency from around 0.5% to 2.2%. This was explained by the combined effect of surface passivation and a build-up of an energy barrier that prevents electron back reactions. It was also found that higher crystallinity of the TiO₂ shells provided better injection and therefore the performance of crystalline shells were clearly better than the amorphous ones.

Finally, the above described core-shell approach has opened up completely new and exciting opportunities for multi-dye DSSCs. Choi *et al.*²⁹ have reported an impressive 8.65% DSSC using a stepwise co-sensitization method in which two organic dyes, complementary in their light absorption, were adsorbed onto TiO₂ separated by a thin Al₂O₃ barrier. First, the TiO₂ films were immersed into a dye absorbing the blue part of the spectrum. The Al₂O₃ intermediate layers were

prepared by dipping of the dyed films into a solution of aluminum 2-propoxide in 2-propanol. After drying, the films were immersed into a dye solution absorbing photons from the red part of the spectrum. The co-sensitized films outperformed both single dye DSSCs clearly demonstrating the huge potential of this approach.

PEM fuel cells

Recently, proton exchange membrane (PEM) fuel cells (Fig. 3) have received increasing attention as they are recognized as a promising potential future power source, in particular for mobile applications. Electrocatalysts (generally Pt-carbon) for PEM fuel cells have to fulfil a primarily requirement – a high specific surface activity, as the catalytic reduction of oxygen (cathode) and the catalytic oxidation of hydrogen/methanol (anode) are surface processes. However, to become commercially viable, PEM fuel cells have to overcome the major barrier of the high electrocatalyst cost caused by the exclusive use of Pt-based catalysts, which is estimated to contribute to as much as 50% of the total PEM fuel cell cost³⁰. Furthermore the lack of stability of the nanodispersed Pt, which is required to maximize the PEM fuel cell performance, and the CO poisoning intrinsic to Pt based cathodes pose a further barrier to PEM fuel cells based on these electrocatalysts. Hence it is important to open up new routes for making low cost and effective catalysts. It is well known that the activity attainable depends significantly on the size of the Pt catalysts³¹ and their support³². Therefore, in order to lower the cost and increase the performance of the catalysts, numerous efforts have focused on the development of (i) novel nanostructures of Pt-based catalysts, and (ii) new nanostructured catalyst supports to replace activated carbons.

The power of a single-cell significantly depends on the specific surface active area of electrocatalysts, determined by the nanostructured electrodes consisting of Pt-catalysts and carbon supports.

Anode reaction: $H_2 \rightarrow 2H^+ + 2e^-$ or $CH_3OH + H_2O \rightarrow CO_2 + 6H^+ + 6e^-$.

Cathode reaction: $O_2 + 4H^+ + 4e^- \rightarrow 2H_2O$.

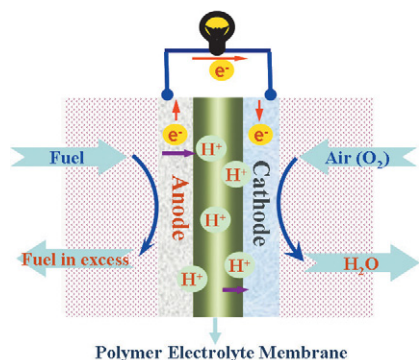


Fig. 3 The schematic of a proton exchange membrane fuel cell showing H^+ ions transfer through proton exchange membrane (PEM) and electrons flow around the external circuit from anode to cathode.

Nanostructured catalysts

Various protocols enabling the synthesis of different Pt nanostructures, such as nanoparticles, nanosphere, and nanowires, have been developed to reduce the size of Pt catalysts in order to maximize the specific surface area of platinum³³⁻³⁵. The activity of the catalysts depends significantly on how well they are distributed over the carbon support. This distribution can be controlled by the mode of synthesis employed, e.g. controlled electrochemical pulse deposition (Fig. 4). Recently, nanostructured platinum alloys have been suggested as alternative catalysts to pure Pt for PEM fuel cells. These materials have a high catalytic activity and improved stability in the fuel cell environment³⁶. The use of these Pt-alloy catalysts, including Pt-Ru, Pt-Fe, Pt-Pb, and Pt-Sn, not only reduce the cost but also improve the performance, by mitigating against CO poisoning, lowering the overpotential, and suppressing Pt dissolution³⁷⁻⁴². Xing *et al.*³⁹ have demonstrated that alloys with a higher Ru content (15 wt %) give a higher and more durable electrocatalytic activity (78 mW/cm²) for methanol oxidation compared to that of lower Ru content alloys (56 mW/cm² for 10 wt %) at 80°C.

Nanostructured carbon supports

The most widely used catalytic support is activated carbon (e.g. carbon black – Vulcan XC 72R). However, the development of more efficient supports is required to prevent detachment and/or aggregation of the Pt catalyst^{43, 44}.

The use of mesoporous carbon (MC), a nanostructured porous material, has proven extremely useful; in contrast to activated carbon black, MC has a large specific surface area with 3D interconnected mesopores, which improves the dispersion of the metal catalysts. Mesoporous carbon electrodes with nanostructured electrocatalysts have exhibited excellent performance in PEM fuel cells⁴⁵⁻⁴⁷.

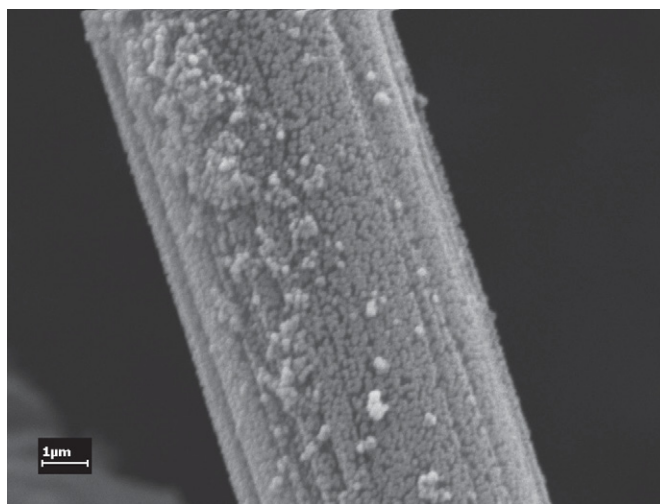


Fig. 4 SEM image of Pt nanoparticles deposited on carbon fibre via controlled electrochemical deposition process.

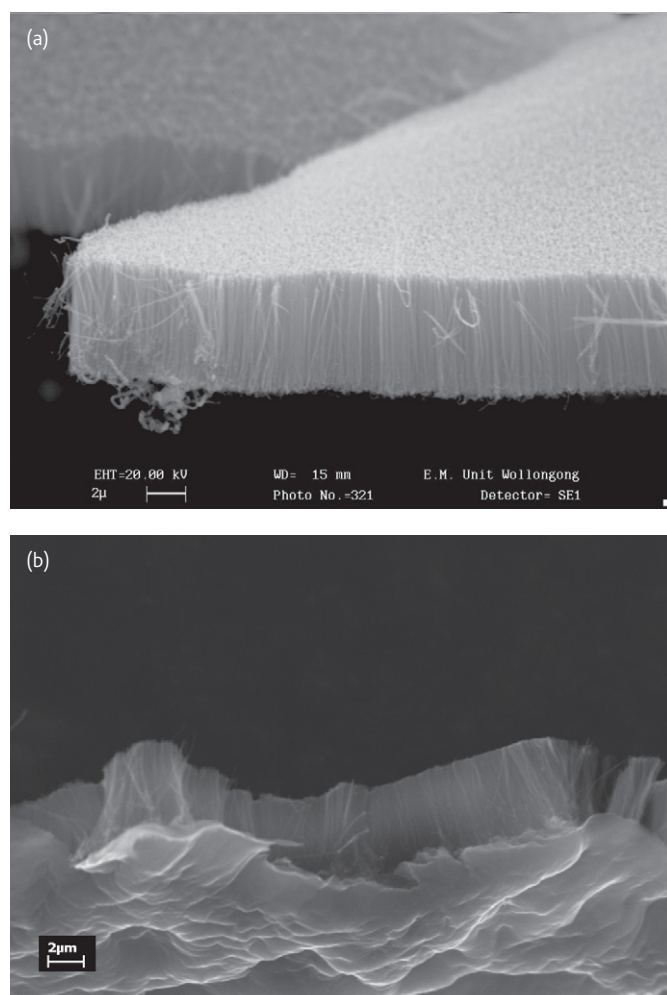


Fig. 5 SEM images of (a) the aligned carbon nanotubes (ACNTs) grown on quartz, (b) the free-standing ACNTs membrane electrode with conductive support.

The other primary carbon-based support material is carbon nanotubes (CNTs)^{48, 49}, which provide a high electrical conductivity and a specific interaction between catalytic metals and the support (i.e. the delocalized π electrons of CNTs and Pt d-electrons), resulting in a higher catalytic activity. The enhancement in performance obtained using nanostructured CNT supports has been widely observed^{50, 51}. There are a few approaches that have been developed to achieve high nano-Pt loading on the CNTs⁵²⁻⁵⁵. The simplest and most widely used approach is the use of *in situ* growth methods. Zheng *et al.*⁵⁶ reported a one-step *in situ* method to disperse Pt nanoparticles on CNTs, using H_2PtCl_6 as a Pt source, ethylene glycol as a reducing agent, and dimethyl formamide (DMF) as a solvent. The resulting Pt/MWNT composites showed a mass specific current density (for methanol oxidation) of 160 mA/mg, which is significantly higher than that of the commercial catalyst E-TEK (82 mA/mg).

The preparation of free-standing conductive CNT-based electrodes is possible^{57, 58}. For example, we developed a novel preparation

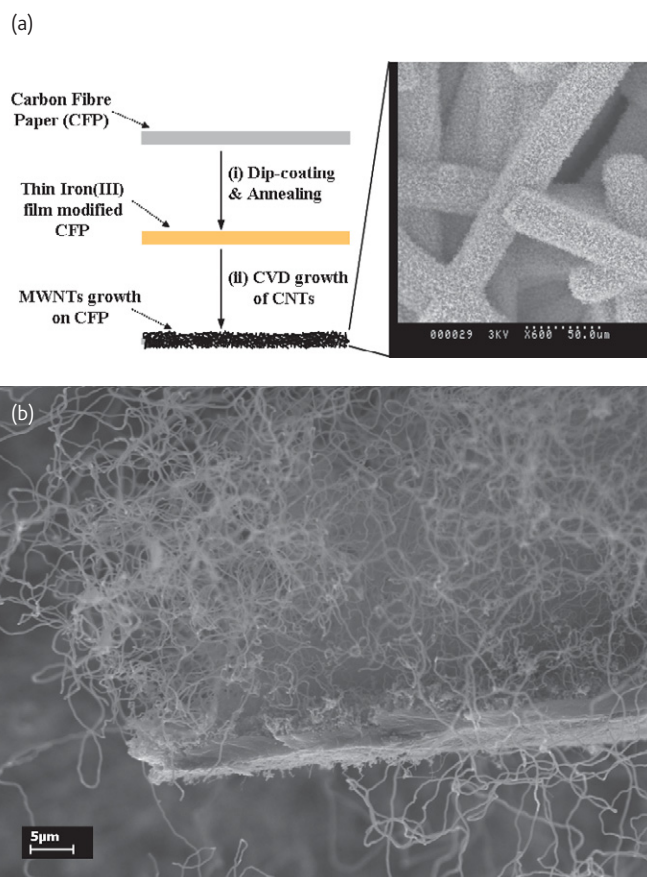


Fig. 6 (a) The schematic on direct growth of CNT NanoWeb on carbon fibre paper; (b) SEM image of CNT NanoWeb modified carbon fibre paper, showing a dense entanglement of CNTs entirely covers the individual carbon fibres whilst still retaining the microporous nature of the host carbon fibre paper, (c) typical SEM image of CNT NanoWeb, consisting of the upper carbon nanotube network and the bottom carbon layer with an obvious intersection.

procedure to produce a free-standing aligned CNT (ACNT) membrane electrode (Fig. 5) used for nano-Pt supports⁵⁸. The so-prepared nano-Pt loaded on ACNT electrode demonstrates a much higher electroactive specific surface area ($143 \pm 14.3 \text{ m}^2 \cdot \text{g}^{-1}$) than mesoporous Pt powders ($60 \text{ m}^2 \cdot \text{g}^{-1}$) or Pt/C ($14-87 \text{ m}^2 \cdot \text{g}^{-1}$) materials, as well as remarkable catalytic activity toward methanol oxidation ($117 \text{ mA} \cdot \text{mg}^{-1}$).

The other approach to solve the problem of adhesion of Pt-CNTs catalysts is to grow carbon nanotubes directly on suitable conductive/metallic substrates^{59, 60} and use them as the nanostructured electrode supports for electrocatalysts. The controlled growth of aligned CNTs onto conducting microsized carbon fibres has been demonstrated⁶¹. However, this method is difficult to scale up in order to match the requirements of electrode dimensions used in PEM fuel cells. Recently, we demonstrated the direct growth of CNTs network (Fig. 6) onto different conducting substrates without the problem of scale up (50 cm^2)^{62, 63}. Following a controlled catalyst loading/dispersion process, these nanosized-catalyst loaded 3D CNT-based electrodes will be ready to use as the catalytic

electrodes in PEM fuel cells. This kind of novel nanostructured electrode has the potential to improve the durability and stability of PEM fuel cell performance.

Other non-carbon catalyst supports (metal oxides) have been used in PEM fuel cell. For example, nanostructured titanium dioxide (TiO_2)⁶⁴ electrodes display high stability when used in a PEM fuel cell as the cathode in acidic environments. Kamat *et al.*⁶⁵ found that the use of nanostructured TiO_2 as a substrate improves the performance of Pt-Ru catalysts for methanol oxidation. Recently, Song *et al.*^{66, 67} demonstrated that the use of TiO_2 nanotube supports for Pt/C enhances the catalytic activity and mitigates against electrode poisoning by CO during methanol oxidation.

A recent exciting development is the cathode based on an intrinsically conductive polymer PEDOT which has been shown to have electrocatalytic activity for oxygen reduction at least matching Pt when a thin layer is deposited onto a porous, breathable polymer substrate such as Goretex⁶⁸. This electrode was shown to be stable to CO poisoning and does not suffer from particle agglomeration. Undoubtedly the nanostructured surfaces encountered at the PEDOT – Goretex interface contributes to this performance.

Nanostructured electrodes for energy storage

Lithium-ion batteries

Commercial Lithium ion batteries have emerged in last decade as one of the great success stories of materials electrochemistry. They can provide high energy density coupled with long cycle life⁶⁹. On charging, Li^+ deintercalates from the cathode material and intercalates into the anode (Fig. 7). Discharge of the battery reverses this process.

The use of nanostructured electrodes in lithium ion batteries (for example, using mesoporous $\beta\text{-MnO}_2$) allows reversible lithium intercalation and deintercalation without destruction of the rutile structure. The use of nanostructures also increases the rate of lithium insertion/removal due to the short lithium ion transport path, enhances electron transport, increases the contact area with the electrolyte and provides an ability to deal with volume changes associated with intercalation⁷⁰.

Cathodes: Lithium transition metal oxides and metal oxides are the two most commonly used cathode materials in lithium ion batteries. Nanostructured LiFePO_4 powders have been used as cathode materials and provide a specific capacity of 125 mAh.g^{-1} and 157 mAh.g^{-1} at discharge rates of 10 C and 1 C with less than 0.08% fade per cycle⁷¹. Nanostructured LiFePO_4/C nanocomposites consisting of monodispersed nanofibers of the LiFePO_4 electrode material mixed with an electronically conductive carbon matrix have also been used as cathode materials. This unique nanocomposite delivers almost 100% of its theoretical discharge capacity at a high discharge rate of 3 C, and 36% of its theoretical capacity at the enormous discharge rate of 65 C. The performance of these

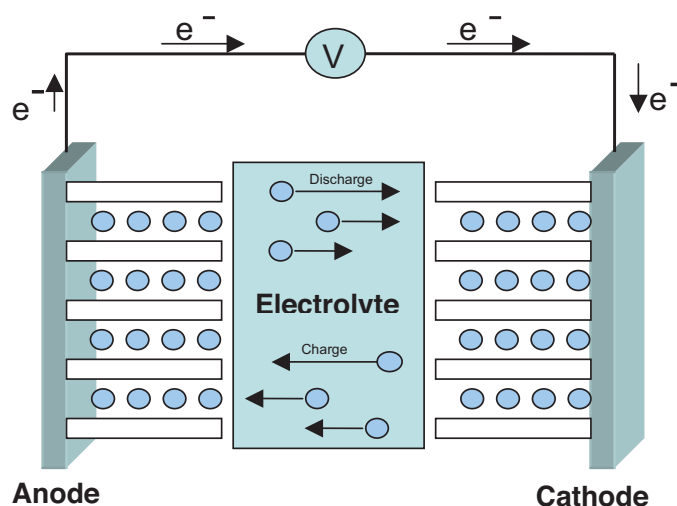


Fig. 7 Schematic representation of the charge/discharge cycle for a lithium-ion battery.

nanocomposite electrodes is attributed to the nanofiber morphology overcoming problems associated with slow Li^+ -transport in the solid state, and the conductive carbon matrix overcomes the inherently poor electronic conductivity of LiFePO_4 ⁷².

Vanadium oxides also have useful properties as lithium cathode materials. Recent work⁷³ has synthesized nanostructured vanadium oxides in the form of nanoribbons and nanowires and shown these to have excellent cycling properties. The material also shows very good cycling properties against ionic liquid electrolytes which hold great promise in improving the safety of lithium ion devices in large scale applications such as electric vehicles⁷⁴.

Recently we have also shown that nanostructured electrodes based on intrinsically conducting polymers (ICP) such as poly(aniline) or poly(methylthiophene) and CNTs are excellent cathode materials for lithium ion and lithium metal batteries⁷⁵. The CNT structure is believed to provide a higher electronic conductivity while the ICP provides the electrochemical process required for the cathode. Battery efficiencies close to 100% with discharge capacities of 120 mAh.g^{-1} were achieved with Li metal and an ionic liquid electrolyte using these composite electrodes.

Anodes

Although the theoretical capacity of metallic anode materials are very high for lithium-ion rechargeable batteries, large volume expansions after the lithiation process results in pulverization of the electrodes⁷⁶. Metal alloys are alternative materials produced when particles of the reactive metal are finely dispersed within a solid mixed-conducting, metallic matrix. The inactive matrix reduces the relative volume expansion of the electrode and serves as a reinforcing material. By reducing the metal alloy particles to nanodimensions the phase transitions becomes more facile and the cracking within the electrode

is reduced even further⁷⁷. A specific capacity of 792 mAh.g⁻¹ has been reported for nanostructured Al_{0.8}Cu_{0.2} with capacity retention of ~50% after 100 cycles⁷⁸.

Carbon nanotubes and nanostructured carbon have been widely studied as anode materials for lithium batteries since their unique structure should allow rapid insertion/deinsertion of lithium ions⁷⁹ as compared to graphite. A specific reversible discharge capacity of 572 mAh.g⁻¹ was obtained for flexible CNT/carbon layer paper⁶² at 0.2 mA.cm⁻². However, surface-layer formation and safety concerns (electroplating of lithium) limit performance of pure CNT materials. Composites of CNTs with Sn and Sn/Sb alloys provide improved charge cycling characteristics⁸⁰.

The low cost of titanium dioxide has attracted the attention of those interested in anode alternatives⁸¹, even though the potentials at which lithium intercalation/deintercalation occur are much higher (for example it is about 1.5 V versus lithium for TiO₂(B)⁸²) than that of carbon materials which are very close to that of Li⁺/Li redox couple. The intrinsic safety advantages comprise the lower overall cell voltage.

Nanostructured TiO₂ accommodates Li by three different mechanisms: insertion into the anatase lattice, double-layer charging and surface-confined charge storage⁸³. A specific capacity of 225 mAh.g⁻¹ was reported for TiO₂(B) nanowires when used as an anode coupled to a LiFePO₄ cathode. An excellent rate capacity was achieved with 80% of the low-rate capacity retained at 5 C⁸⁴. The retention of nanowire morphology on extended cycling and intercalation/deintercalation result in excellent rate capacity and good cycle life. Recently an initial discharge capacity of 357 mAh.g⁻¹ was reported for titanium dioxide nanosheets⁸⁵.

Supercapacitors

Supercapacitors, so called electrochemical capacitors, possess much higher power densities (> 500 W.kg⁻¹), excellent reversibility, and longer cycle life (> 10⁵ cycles) compared with rechargeable batteries⁸⁶. Supercapacitors store energy using either ion adsorption (electrochemical double layer capacitors, EDLCs) or fast surface redox reactions (pseudo-capacitors). Nanostructured carbonaceous materials with high surface area are commonly used for EDLCs. Transition metal oxides as well as conducting polymers are widely studied materials for use as electrodes in pseudo-capacitors⁸⁷.

The use of carbon nanotubes for supercapacitor electrodes provides a network of mesopores formed by nanotube entanglement. This provides an easily accessible electrode-electrolyte interface⁸⁸. Improved capacity can be achieved by creating a nanocomposite with conducting polymers⁸⁹.

Carbon-nanotube aerogel electrodes exhibit remarkable supercapacitor performance, with a specific capacitance of 524 F.g⁻¹ compared with a capacitance of 320 F.g⁻¹ for activated carbon. This

capacitor performance can be attributed to the high specific surface area of the aerogel electrodes⁹⁰.


Hydrous ruthenium oxide is a most promising electrode material due to the ultrahigh pseudocapacitance and the excellent cycle stability attainable. In an aqueous H₂SO₄ electrolyte a specific capacitance of 720 F.g⁻¹ was achieved⁹¹. The use of a 3D, arrayed, nanotubular architecture based on hydrous ruthenium oxide exhibited a very high specific power and energy density of 4320 kW.kg⁻¹ and 7.5 Wh.kg⁻¹ respectively⁹². However, ruthenium oxide is very expensive and so the use of other nanostructured materials, iron oxide, manganese oxide and nickel oxide has attracted attention. Highly porous nanostructured iron oxide films exhibited a specific capacitance of 173 F.g⁻¹ at 3 A.g⁻¹ charge/discharge⁹³. The large pores (randomly distributed nanosheets) within the iron oxide are large enough to maintain the high rate charging/discharging.

The specific capacitance of CNT electrodes are remarkably enhanced with a thin layer of conducting polymer coating due to the contribution of the pseudo-faradaic properties from polymer⁹⁴.

Nanostructured conducting polymers may be prepared using either template-assisted or non template-assisted methods⁹⁵. For example, templates with cylindrical pores of uniform diameter have been used and nanofibril or nanotubule conducting polymers deposited within the pores⁹⁶. PEDOT-nanotube-based supercapacitors can achieve a high power density of 25 kW.kg⁻¹. This is attributed to the fast charge/discharge of nanotubular structures: hollow nanotubes allow counterions to readily penetrate into the polymer and access the internal surface, while the thin wall provides a short diffusion distance to facilitate ion transport⁹⁷. Large arrays of oriented PANI nanowires exhibited capacitance values several times higher than bulk polymer⁹⁸.

Conclusions and future developments

Energy conversion and storage are areas of research foremost in the minds of the scientific and general communities. It is critical that we continue to develop alternative energy conversion strategies and device more efficient energy storage and recovery systems. The advent of nanotechnology and the materials synthesis and characterisation tools that have emerged under this umbrella place us in an exciting era.

There is no doubt that as our ability to assemble more efficient, more robust nanostructured electrodes with predetermined compositions, continues to improve so also will the performance of the energy conversion and storage systems that utilise these compounds. 

Acknowledgements

The authors are grateful to the ARC for funding under the ARC Centre of Excellence program and the ARC Federation Fellowship program (Gordon Wallace, Doug MacFarlane).

REFERENCES

- 1 Smalley, R. E., *MRS Bulletin* (2005) **30**, 412.
- 2 Zweibel, K., *The terawatt challenge for thin film photovoltaics*, in *Thin Film Solar Cells*, eds. Poortmans, J., and Arkhipov, V., J. Wiley & Sons Ltd (2006).
- 3 Würfel, P., *Physics of Solar Cells: From Principles to New Concepts*, Wiley-VCH Verlag GmbH & Co. KGaA, Weinheim (2005).
- 4 Brabec, C. J., et al., *Adv. Funct. Mater.* (2001) **11**, 15.
- 5 Grätzel, M., *Nature* (2001) **414**, 338.
- 6 Padinger, F., et al., *Adv. Funct. Mater.* (2003) **13**, 1.
- 7 Shaheen, S. E., et al., *Appl. Phys. Lett.* (2001) **78**, 841.
- 8 Halls, J. M., et al., *Appl. Phys. Lett.* (1996) **68**, 3120.
- 9 Nazeeruddin, M. K., et al., *J. Am. Chem. Soc.* (2005) **127**, 16835.
- 10 Campbell, W. M., et al., *J. Phys. Chem. C* (2007) **111**, 11760.
- 11 O'Regan, B., and Grätzel, M., *Nature* (1991) **353**(6346), 737.
- 12 Grätzel, M., *J. Photochem. Photobiol., A* (2004) **164**, 3.
- 13 Hoppe, H., et al., *Adv. Funct. Mater.* (2004) **14**, 1005.
- 14 Van Bavel, S. S., et al., *Nano Lett.* (2009) **9**(2), 507.
- 15 Ma, C.-Q., et al., *Angew. Chem. Int. Ed.* (2007) **46**, 1679.
- 16 Ma, C.-Q., et al., *Adv. Funct. Mater.* (2008) **18**, 3323.
- 17 Scherf, U., et al., *Acc. Chem. Res.* (2008) **41**(9), 1086.
- 18 Cravino, A., and Sariciftci, N. S., *J. Mater. Chem.* (2002) **12**, 1931.
- 19 Cravino, A., and Sariciftci, N. S., *Nat. Mater.* (2003) **2**, 360.
- 20 Ito, S., et al., *Thin Solid Films* (2008) **516**, 4613.
- 21 Chen, D., et al., *Adv. Mater.* (2009) **21**, 1.
- 22 Martinson, A. B. F., et al., *Nano Lett.* (2007) **8**, 2183.
- 23 Mor, G. K., et al., *Nano Lett.* (2006) **2**, 215.
- 24 Law, M., et al., *J. Phys. Chem. B* (2006) **110**, 22652.
- 25 Kuang, D., et al., *ACS Nano* (2008) **6**, 1113.
- 26 Zaban, A., et al., *Chem. Commun.* (2000), 2231.
- 27 Kay, A., and Grätzel, M., *Chem. Mater.* (2002) **14**, 2930.
- 28 Suntola, T., and Simpson, M., *Atomic Layer Epitaxy*, Chapman & Hall (1990).
- 29 Choi, H., et al., *Angew. Chem. Int. Ed.* (2008) **47**, 8259.
- 30 Gasteiger, H. A., et al., *Appl. Catal. B: Environ.* (2005) **56**, 9.
- 31 Kinoshita, K., *J. Electrochem. Soc.* (1990) **137**, 845.
- 32 Shao, Y. Y., et al., *J. Power Sources* (2007) **171**, 558.
- 33 Liang, H. P., et al., *Angew. Chem. Int. Ed.* (2004) **43**, 1540.
- 34 Tian, N., et al., *Science* (2007) **316**, 732.
- 35 Wieckowski, A., Savinova, E. R., and Vayenas, C. G., *Catalysis and electrocatalysis at nanoparticle surfaces*, Marcel Dekker, New York (2003).
- 36 Costamagna, P., and Scrinivason, S., *J. Power Sources* (2001) **102**, 242.
- 37 Switzer, E. E., and Datye, A. K., *Top Catal.* (2007) **46**, 334.
- 38 Jiang, J., and Kucernak, A., *Electrochem. Commun.* (2009) **11**, 623.
- 39 Xu, W., et al., *J. Phys. Chem. B* (2005) **109**(30), 14325.
- 40 Atassi, A., et al., *J. Appl. Electrochem.* (2006) **36**, 1143.
- 41 Yang, S., et al., *Adv. Funct. Mater.* (2008) **18**, 2745.
- 42 Guo, Y. G., et al., *Adv. Mater.* (2005) **17**, 746.
- 43 Liu, J. G., et al., *Phys. Chem. Chem. Phys.* (2004) **6**, 134.
- 44 Shao, Y., et al., *J. Power Sources* (2007) **167**, 235.
- 45 Chai, G. S., et al., *J. Phys. Chem. B* (2004) **108**, 7074.
- 46 Nakagawa, N., et al., *Electrochem.* (2007) **75**, 172.
- 47 Wang, Y. G., et al., *Chem. Mat.* (2007) **19**, 2095.
- 48 Serp, P., et al., *Appl. Catal. A: Gen.* (2003) **253**, 337.
- 49 Lee, J., et al., *Adv. Mater.* (2006) **18**, 2073.
- 50 Wildgoose, G. G., et al., *Small* (2006) **2**, 182.
- 51 Lee, K., et al., *J. Appl. Electrochem.* (2006) **36**, 507.
- 52 Kumar, M. K., and Ramaprabhu, S., *J. Phys. Chem. B* (2006) **110**(23), 11291.
- 53 Okamoto, M., et al., *Small*, doi:10.1002/smll.200801742.
- 54 Paoletti, C., et al., *J. Power Sources* (2008) **183**, 84.
- 55 Rajalakshmi, N., and Dhathathreyan, K. S., *Inter. J. Hydrogen Energy* (2008) **33**, 5672.
- 56 Zheng, S. F., et al., *J. Phys. Chem. C* (2007) **111**, 11174.
- 57 Gong, K., et al., *Science* (2009) **323**, 760.
- 58 Liu, Y., et al., *Chem. Mater.* (2008) **20**(8), 2603.
- 59 Bordjiba, T., et al., *Chem. Phys. Lett.* (2007) **441**, 88.
- 60 Park, D., et al., *J. Mat. Sci.* (2003) **38**, 4923.
- 61 Qu, L., et al., *Small* (2006) **2**(8-9), 1052.
- 62 Chen, J., et al., *Adv. Mater.* (2008) **20**, 566.
- 63 Chen, J., et al., *Energy Environ. Sci.*, doi:10.1039/b816135f.
- 64 Kraemwer, S. V., et al., *J. Power Sources* (2008) **180**, 185.
- 65 Drew, K., et al., *J. Phys. Chem. B* (2005) **109**, 11851.
- 66 Song, H., et al., *J. Power Sources* (2007) **170**, 50.
- 67 Song, H., et al., *J. Power Sources* (2008) **178**, 97.
- 68 Winther-Jensen, B., et al., *Science* (2008) **321**, 671.
- 69 David Linden, *Handbook of batteries (3rd ed.)*, McGraw-Hill, New York, London (2002).
- 70 Bruce, P. G., et al., *Angew. Chem. Int. Ed.* (2008) **47**, 2930 (references herein).
- 71 Choi, D., and Kumta, P. N., *J. Power Sources* (2007) **163**, 1064.
- 72 Sides, C. R., et al., *Electrochem. Solid State Lett.* (2005) **8**, A484.
- 73 Chou, S. L., et al., *Chem. Mater.* (2008) **20**, 7044.
- 74 Armand, M., et al., *Nat. Mater.*, in press.
- 75 Sivakkumar, S. R., et al., *J. Electrochem. Soc.* (2007) **154**, A834.
- 76 Wang, C., et al., *J. Power Sources* (2001) **93**, 174.
- 77 Aricò, A. S., et al., *Nat. Mater.* (2005) **4**, 366.
- 78 Wang, C. Y., et al., *J. Electrochem. Soc.* (2008) **155**, 615.
- 79 Frackowiak, E., et al., *Carbon* (1999) **37**, 61.
- 80 Park, M. S., et al., *Chem. Mater.* (2007) **19**, 2406.
- 81 Bavykin, D. V., et al., *Adv. Mater.* (2006) **18**, 2807.
- 82 Armstrong, A. R., et al., *Adv. Mater.* (2005) **17**, 862.
- 83 Kavan, L., et al., *Chem. Mater.* (2004) **16**, 477.
- 84 Armstrong, G., et al., *Adv. Mater.* (2006) **18**, 2597.
- 85 Tsai, M. C., et al., *Chem. Mater.* (2009) **21**, 499.
- 86 Conway, B. E., *Electrochemical Supercapacitors: Scientific Fundamentals and Technological Applications*, Kluwer Academic/Plenum Publisher, New York (1999).
- 87 Simon, P., and Gogotsi, Y., *Nat. Mater.* (2008) **7**, 845.
- 88 Frackowiak, E., and Béguin, F., *Carbon* (2002) **40**, 1775.
- 89 Sivakkumar, S. R., et al., *J. Power Sources* (2007) **171**, 1062.
- 90 Bordjiba, T., et al., *Adv. Mater.* (2008) **20**, 815.
- 91 Zheng, J. P., and Low, T. R., *J. Electrochem. Soc.* (1995) **142**, L6.
- 92 Hu, C. C., et al., *Nano Lett.* (2006) **6**, 2690.
- 93 Wu, M. S., et al., *Electrochem. Solid-state Lett.* (2009) **12**, A1.
- 94 Hughes, M., et al., *Chem. Mater.* (2002) **14**, 1610.
- 95 Wallace, G. G., and Innis, P. C., *J. Nanosci. Nanotech.* (2002) **5**, 441.
- 96 Martin, C. R., *Science* (1994) **266**, 1961.
- 97 Liu, R., et al., *Nanotechnol.* (2008) **19**, 21570.
- 98 Zou, X., et al., *J. Solid State Electrochem.* (2007) **11**, 317.